Supporting Information

In situ Conversion Reaction of Magnesium Fluoride to Boost the Performance of Sulfide-Based Electrolyte Li_6PS_5Cl for All-Solid-State Lithium Metal Batteries

Yuzhe Zhang[#[a]], Haolong Chang[#[a]], Xiaohu Hu[[a]], Shijie Xu[[a]], Xinyu Wang[[a]], Shunjin Yang[[a]], Yujiang Sun[[a]], Xiao Sun[[a]], Dehang Ren[[a]], Xing Chen[*[a,b]], Fangyi Cheng[[c]], Yongan Yang[*[a,b,c]]

[a]Institute of Molecular Plus, Department of Chemistry, School of Chemical Engineering and Technology, Tianjin University, Tianjin 300072, China.

[b]Haihe Laboratory of Sustainable Chemical Transformations, Tianjin 300192, China.

[c]Key Laboratory of Advanced Energy Materials Chemistry (Ministry of Education), College of Chemistry, Nankai University, Tianjin 300071, China.

#These authors contributed equally to this work.

*Corresponding Authors: X. Chen (xing_chen@tju.edu.cn); Y. Yang (revned_yang@tju.edu.cn).

1. Experimental Section

1.1 Preparation of Li_6PS_5Cl-MgF_2

Firstly, the MgF_2 powder was ball milled for 20 min to make finer powder by using a bead-to-material weight ratio of 15:1. Next, the obtained MgF_2 and commercial Li_6PS_5Cl (99%, Guangdong Mache Power Technology Co., Ltd, China) at a certain mass ratio were put in an agate mortar and manually ground for 10 min. According to the weight fraction of MgF_2, three sets of samples were prepared and marked as

Li_6PS_5Cl-MgF_2(4 wt%), Li_6PS_5Cl-MgF_2(7 wt%) and Li_6PS_5Cl-MgF_2(10 wt%). The entire preparation process was carried out in an argon protected glove box. Besides, three other metal fluorides (AlF_3, ZnF_2 and SnF_2) with the mass fraction of 7 wt% were also used to make composite electrolytes.

1.2 Characterization

X-ray diffraction (XRD, Rigaku Smartlab9KW, Japan) was used to analyze crystalline phases of solid electrolytes (SEs) using Cu K_α radiation. The scanning range was $2\theta = 10° - 60°$ with a scan rate of 20°/min. The XRD samples were prepared by spreading powdery materials onto glass substrates, which were covered with an arch-shaped polyamide film to protect materials from air exposure. Field emission scanning electron microscope (FESEM, Apreo S LoVac, Czech) was performed to observe morphologies of SEs. High-resolution transmission electron microscope (HRTEM, Thermo Scientific Talos F200X, America) with energy dispersive X-Ray spectroscopy (EDS) function was employed to further characterize morphologies and elemental composition of SEs. The valence states of elements in SEs were analyzed using X-ray photoelectron spectroscopy (XPS, ESCALAB-Xi, English).

1.3 Electrochemical Tests

1.3.1 Measurement of Ionic Conductivity and Electronic Conductivity

Firstly, 130 mg of SE was placed into a polyaldehyde mold (10 mm diameter) and pressed with two stainless steel rods at 360 MPa. Second, the mold was fastened with

four screws, with two stainless steel rods inserted into the polyaldehyde mold to serve as current collectors. Third, the assembled mold batteries were put into an oven for ionic conductivity tests. For obtaining the ionic conductivity, electrochemical impedance spectra were measured on an electrochemical workstation (SP-200, BioLogic Science Instruments Co., Ltd, China) from 0.1 Hz to 7×10^6 Hz with a voltage amplitude of 5 mV. For measuring the electronic conductivity, chronoamperometry at the test voltage of 1 V was used to collect the current-time curves. The ionic conductivity and electronic conductivity of SEs were calculated according to **Eqn. (1)**:

$$\sigma = d/AR \quad (1)$$

where σ is ionic/electron conductivity, d is the thickness of electrolyte layer, A is the area of electrolyte layer and R is the resistance of SE layer.

1.3.2 Assembly of Lithium Metal Symmetric Batteries

Firstly, 130 mg of SE was placed into a polyaldehyde mold (10 mm diameter) and pressed with two stainless steel rods at 240 MPa for 15 s. Secondly, a piece of lithium foil was pressed on both sides of SEs layer under a pressure of 60 MPa for 30 s. Finally, the mold battery was fastened with screws to maintain a constant pressure of 10 MPa and placed into an oven kept at 30℃ for electrochemical measurements.

1.3.3. Assembly of Batteries for CV Tests

The SE powder and Ketjen black (Lion Corporation, Japan) were placed in an agate mortar with a mass ratio of 4:1, and then manually ground for 10 min for later

use. After pressing the electrolyte layer using the same step in 1.3.2, 10 mg of the premade mixture was spread on the SE layer and pressed under 720 MPa for 30 s. Then, the lithium foil was pressed on the other side of SE layer under 60 MPa for 30 s. Finally, the mold battery was fastened with screws and placed into an oven kept at 30℃ for CV test. CV tests were measured in the voltage range of 0.01 - 0.65 V and 0.65 - 5 V at a scan rate of 1 mV/s.

1.3.4 Assembly of All-Solid-State Lithium Batteries

Firstly, the SE layer was prepared under 240 MPa for 15 s. Secondly, NCM721 and Li_6PS_5Cl were placed into an agate mortar with a mass ratio of 7:3 and ground for 5 min. Thirdly, 5 mg of the above mixture was spread on the prepared electrolyte layer and pressed under 720 MPa for 30 s. Fourthly, the lithium foil (thickness of about 85 μm) was pressed on the other side of SE layer under 60 MPa for 30 s. Finally, the mold battery was fastened with screws and put into an oven kept at 30℃ or 60℃. Galvanostatic discharge/charge measurements were carried out in the voltage range of 2.6 V - 4.35 V on Land CT-2001A battery analyzers.

2. Computational Section

Stationary points on the reaction pathways were calculated using spin-polarized density functional theory (DFT) with Perdew-Burke-Ernzerhof (PBE) type exchange–correlation functional[1] within generalized gradient approximation[2] in Vienna *ab initio* simulation package (VASP 6.3.2)[3,4]. The cutoff energy of plane-wave basis set is 450

eV and 3×3×1 Gamma k-points in the first Brillouin zone and the projector augmented wave (PAW) methods were employed[5]. For geometry optimization, the atomic structures are fully relaxed until the force on each atom is less than 0.02 eV $Å^{-1}$ and energy change between two self-consistent steps is smaller than 10^{-5} eV. The van der Waals (vdW) interaction was taken into account by DFT-D3 method[6]. To avoid inter-layer interaction, a vacuum layer more than 15 Å in the Z-direction is considered. And transition states are searched by the climbing image nudged elastic band method (CI-NEB)[7]. Charge density differences and spin densities were obtained using VASPKIT package[8].

References

1. J. P. Perdew, M. Ernzerhof, K. Burke, Rationale for mixing exact exchange with density functional approximations, *J. Chem. Phys.*, 1996, **105**, 9982-9985.

2. J. P. Perdew, K. Burke, M. Ernzerhof, Generalized gradient approximation made simple, *Phys. Rev. Lett.*, 1996, **77**, 3865-3868.

3. G. Kresse, J. Furthmüller, Efficiency of ab-initio total energy calculations for metals and semiconductors using a plane-wave basis set, *Comput. Mater. Sci.*, 1996, **6**, 1550.

4. G. Kresse, J. Furthmüller, Efficient iterative schemes for ab initio total-energy calculations using a plane-wave basis set, *Phys. Rev. B*, 1996, **54**, 11169-11186.

5. G. Kresse, D. Joubert, From ultrasoft pseudopotentials to the projector augmented-wave method, *Phys. Rev. B*, 1999, **59**, 1758-1775.

6. S. Grimme, J. Antony, S. Ehrlich, H. Krieg, A consistent and accurate ab initio

parametrization of density functional dispersion correction (DFT-D) for the 94 Elements H-Pu, *J. Chem. Phys.*, 2010, **132**, 154104.

7. G. Henkelman, B. P. Uberuaga, H. Jónsson, A climbing image nudged elastic band method for finding saddle points and minimum energy paths, *J. Chem. Phys.*, 2000, **113**, 9901-9904.

8. V. Wang, N. Xu, J. C. Liu, G. Tang, W. T. Geng, VASPKIT: A user-friendly interface facilitating high-throughput computing and analysis using VASP Code, *Comput. Phys. Commun.*, 2021, **267**, 108033.

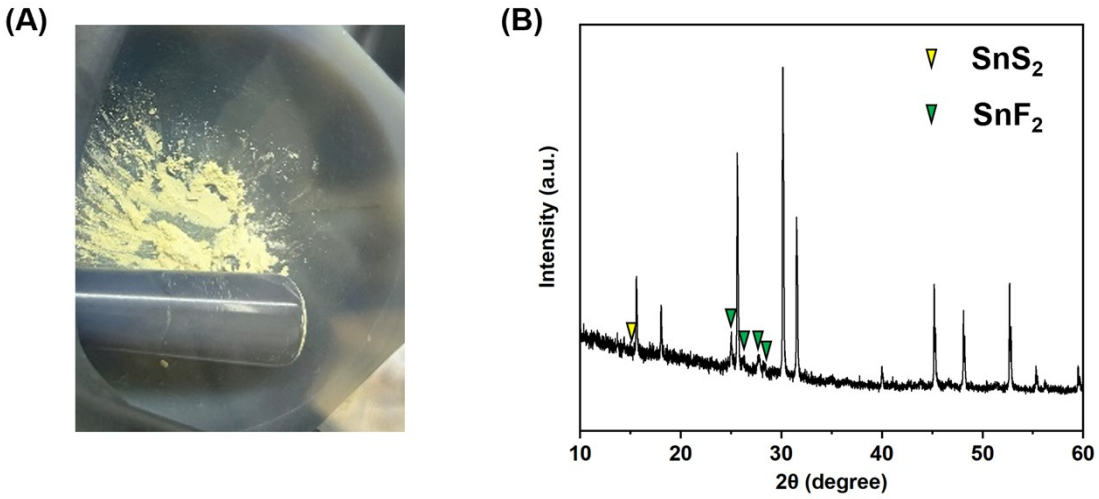

Fig. S1. (A) Optical image of SnF_2 and Li_6PS_5Cl after manual grinding, (B) XRD pattern of Li_6PS_5Cl-SnF_2 composite electrolytes.

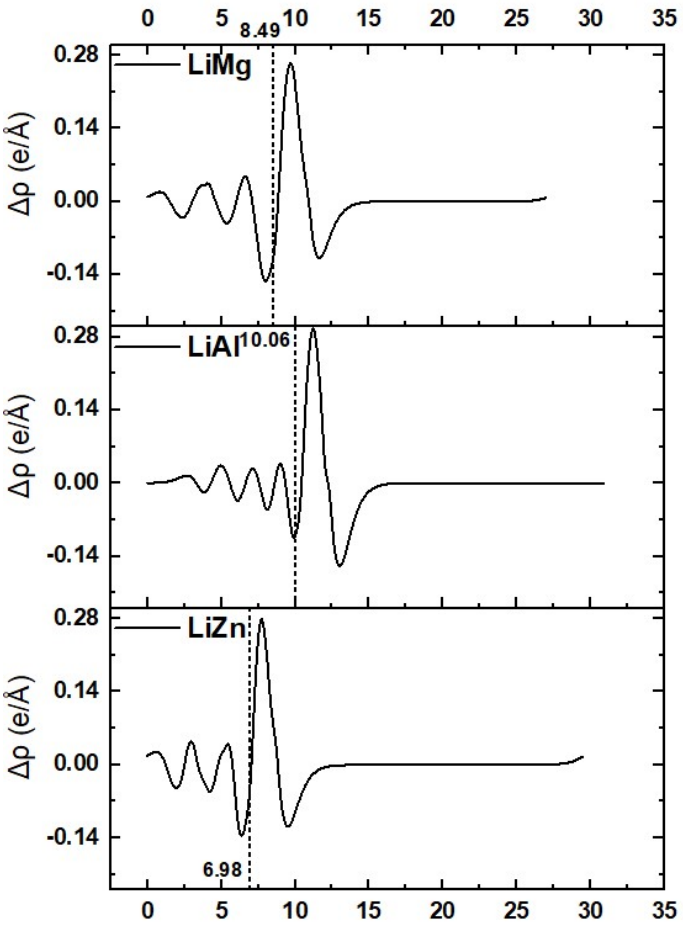

Fig. S2. The charge distribution of Li-LiMg(100), Li-$LiAl_3$(100) and Li-LiZn(100) along the z-axis direction.

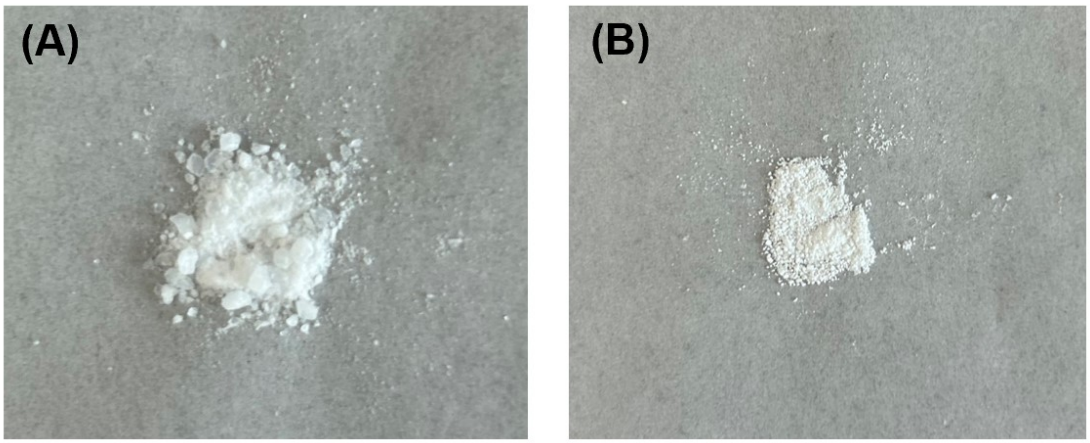

Fig. S3. (A) Optical image of pristine MgF_2 particles, (B) Optical image of MgF_2 particles after ball milling.

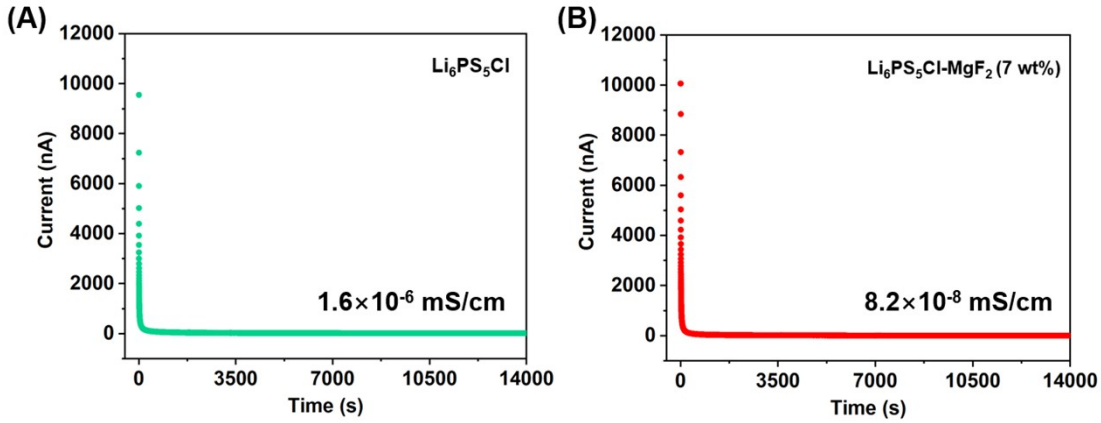

Fig. S4. The chronoamperometric (current-time) profiles for extracting electronic conductivity of (A) Li_6PS_5Cl and (B) Li_6PS_5Cl-MgF_2(7 wt%).

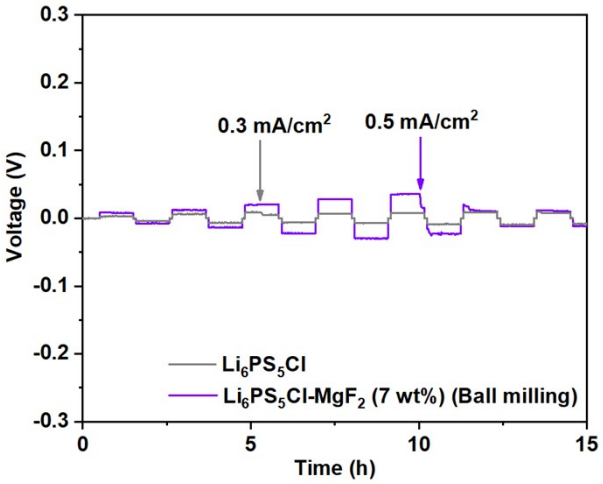

Fig. S5. CCD curves of Li|Li_6PS_5Cl (ball milling)|Li and Li|Li_6PS_5Cl-MgF_2(7 wt%) (ball milling)|Li cells at 30°C.

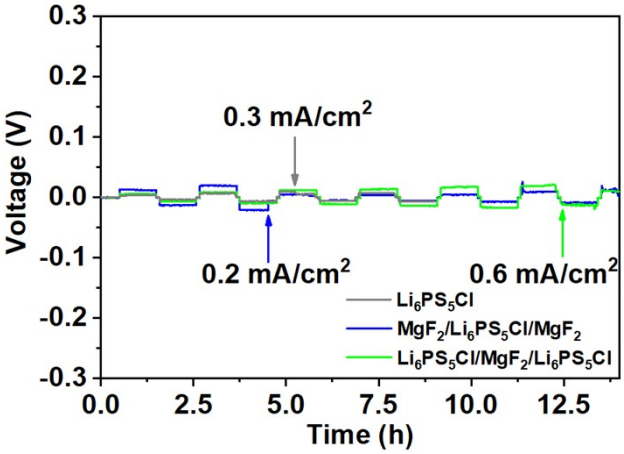

Fig. S6. CCD curves of Li symmetric cells at 30℃ for three different electrolytes of Li_6PS_5Cl, $MgF_2/Li_6PS_5Cl/MgF_2$, and $Li_6PS_5Cl/MgF_2/Li_6PS_5Cl$.

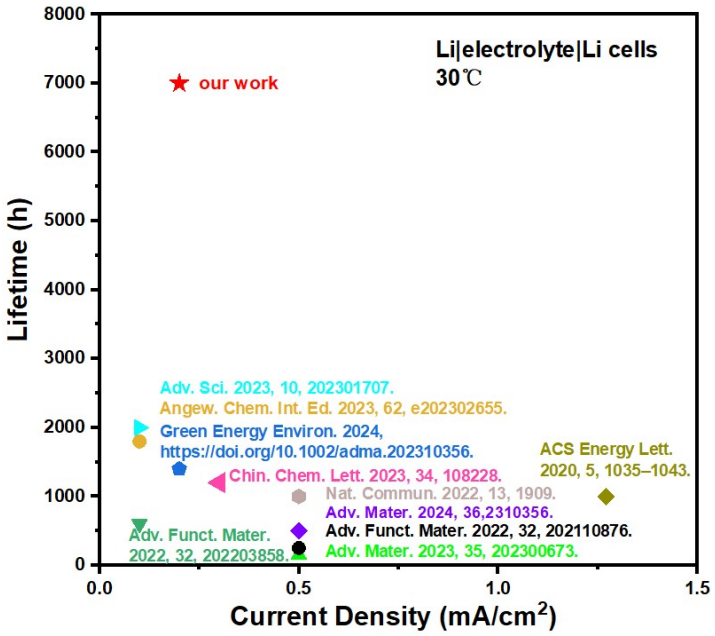

Fig. S7. Performance comparison of lithium symmetric cells between our Li_6PS_5Cl-MgF_2(7 wt%) composite electrolyte with relevant studies in literature.

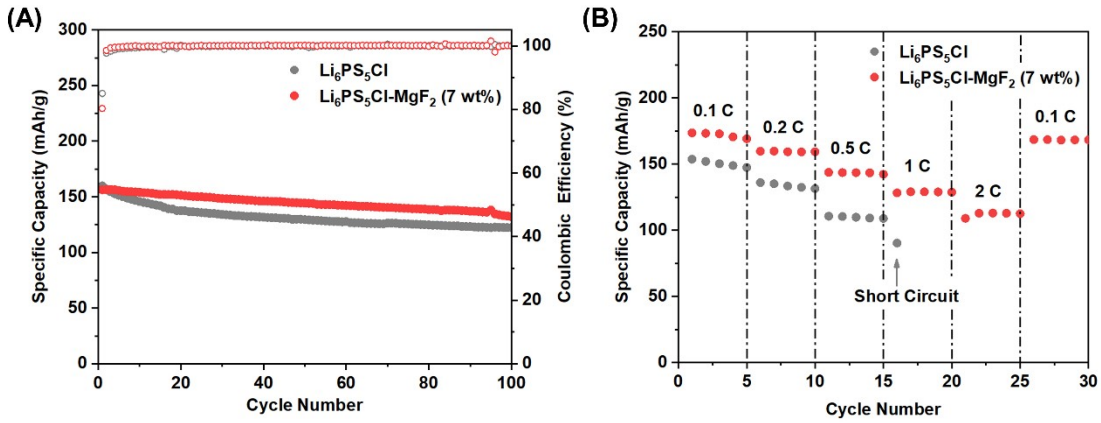

Fig. S8. (A) Cycling stability of Li|electrolyte|NCM721 full cells at 60°C and 0.2 C, (B) Rate capability of Li|electrolyte|NCM721 full cells at 60°C.

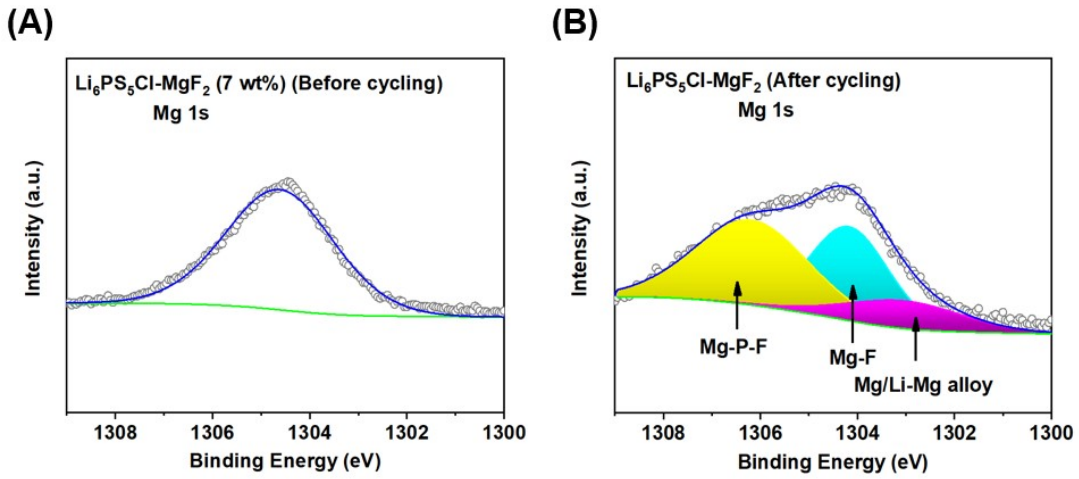

Fig. S9. XPS spectra for Mg 1s of Li_6PS_5Cl-MgF_2 in Li|Li_6PS_5Cl-MgF_2(7 wt%)|Li cell before (A) and after cycling (B).